

Dynamical Spin-Orbit Coupling of a Quantum Gas

Ronen M. Kroese,^{1,2} Yudan Guo,^{1,2} and Benjamin L. Lev^{1,2,3}

¹*Department of Physics, Stanford University, Stanford, California 94305, USA*

²*E. L. Ginzton Laboratory, Stanford University, Stanford, California 94305, USA*

³*Department of Applied Physics, Stanford University, Stanford, California 94305, USA*



(Received 15 April 2019; published 18 October 2019)

We realize the *dynamical* 1D spin-orbit coupling (SOC) of a Bose-Einstein condensate confined within an optical cavity. The SOC emerges through spin-correlated momentum impulses delivered to the atoms via Raman transitions. These are effected by classical pump fields acting in concert with the quantum dynamical cavity field. Above a critical pump power, the Raman coupling emerges as the atoms superradiantly populate the cavity mode with photons. Concomitantly, these photons cause a backaction onto the atoms, forcing them to order their spin-spatial state. This SOC-inducing superradiant Dicke phase transition results in a spinor-helix polariton condensate. We observe emergent SOC through spin-resolved atomic momentum imaging and temporal heterodyne measurement of the cavity-field emission. Dynamical SOC in quantum gas cavity QED, and the extension to dynamical gauge fields, may enable the creation of Meissner-like effects, topological superfluids, and exotic quantum Hall states in coupled light-matter systems.

DOI: 10.1103/PhysRevLett.123.160404

Quantum simulation in the ultracold atomic physics setting has been enriched by techniques using laser-induced atomic transitions to create synthetic gauge fields [1–3], including spin-orbit coupling (SOC) [4]. Quantum gases in synthetic gauge fields may allow the creation of exotic quantum phases such as topological superfluids in a pristine environment [3,5,6]. At the same time, strong and tunable atom-atom interactions mediated by cavity QED light-matter coupling has introduced new capabilities into quantum simulation [7–11]. As such, many-body cavity QED provides unique opportunities for exploring quantum phases and transitions away from equilibrium [8,12–15].

Our work combines these two techniques—many-body cavity QED and synthetic gauge fields—for the creation of a novel quantum system exhibiting dynamical spin-orbit coupling. We experimentally demonstrate the emergence of SOC in a Bose-Einstein condensate (BEC) via the use of a cavity field possessing its own quantum dynamics. Our experiment realizes key aspects of several (previously unrealized) theoretical proposals for creating exotic quantum many-body states via cavity-induced dynamical gauge fields, including SOC [16–29]. By doing so, this work opens avenues toward observing exotic phenomena predicted in these works as well as the creation of dynamical gauge fields, complementing recent progress demonstrating density-dependent gauge fields using optical lattices [30,31]. Specifically, one might be able to explore unusual nonlinear dynamics [19], novel cooling effects in cavity optomechanics [32], striped and quantum Hall-like phases [16,17,21], artificial Meissner-like effects [28,33], exotic magnetism [18,34], and topological superradiant states

[35–37]. Adding intracavity optical lattices could create states with directed transport, chiral liquids, and chiral insulators [23–26,28].

Static SOC has been realized in free-space Bose and Fermi quantum gases using two-photon Raman transitions between atomic spin states [4,38–41], where the two lasers forming the Raman transition are in classical coherent states with externally fixed intensity. The Raman transition realizes SOC by transferring a recoil momentum to each atom as the spin is flipped, with the recoil direction being correlated with the spin state. The key to our dynamical SOC realization is the replacement of one of these classical fields with a cavity mode; see Figs. 1(a) and 1(b). Vacuum fluctuations of the cavity mode stimulate Raman scattering of the pump into this mode. The scattering rate is slow while the atomic spins and positions are disordered. However, at sufficiently high external pump power, the scattering becomes superradiant due to atomic ordering into a jointly organized spin *and* motional state, reflecting the spin-orbit coupled nature of the system. Because the cavity field feeds back onto the atoms, the scattering process generating the SOC is dynamical: the SOC depends on the spatial and spin organization of the atoms and vice versa.

In contrast to systems with standing-wave pump fields in which no SOC arises [42], SOC emerges at the transition threshold when running-wave fields are used as pumps. This is because the running-wave pumps, in conjunction with the cavity mode, impart momentum kicks to the atoms as they flip the atomic spins [44]. Momentum is transferred only along the pump axis because the cavity field is a standing wave. Figure 2 depicts the emergence of SOC, both in terms of occupation of momentum states and in the

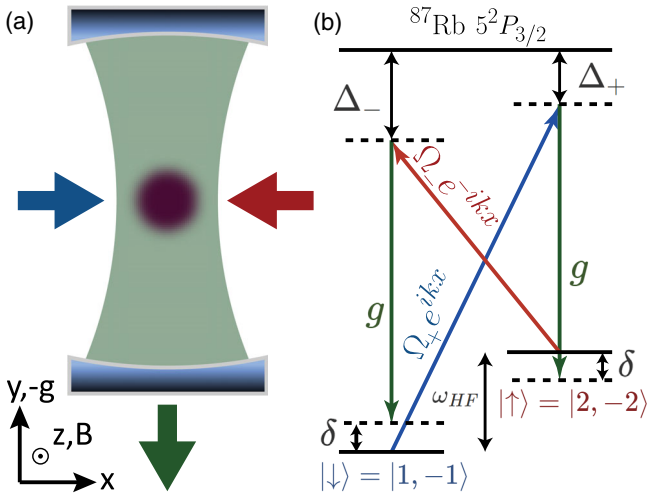


FIG. 1. (a) Schematic of the experiment. Two Raman pump beams (red and blue arrows), polarized along the cavity axis, counterpropagate through a BEC of Rb (purple) inside a TEM₀₀ cavity. The cavity emission (green arrow) is detected by a single-photon counter, and the atoms are imaged in time of flight by a CCD camera (not shown). (b) Level diagram illustrating the cavity-assisted Raman coupling between two hyperfine levels of ⁸⁷Rb acting as the spin states. The counterpropagating running-wave nature of the pumps is explicitly notated by $e^{\pm ikx}$. See text for definitions of all quantities.

coupling between the bands. The phase transition results in a spinor-helixlike state where the spin state rotates along \hat{x} with a period commensurate with the pump wavelength. While the total density remains translationally invariant along \hat{x} , both spin and density are modulated along the cavity axis, as described below.

This dynamical SOC may also be understood from the perspective of cavity-field phase fluctuations. Below threshold, the scattering into the cavity is due to the pump light coupling to incoherent atomic spin and density wave fluctuations [43]. These spinor density-wave fluctuations cause the resonating light to possess a phase that is both uncorrelated and time varying with respect to that of the pump field. Therefore, coherent Raman transitions—and thus, SOC—are suppressed due to the random diffusion of the relative phase between the pump and cavity fields.

Stable SOC emerges only once the phase of the cavity field locks with respect to the pump fields. This locking occurs when the pump power reaches a threshold for triggering a nonequilibrium (Hepp-Lieb) Dicke superradiant phase transition [8,15]. At threshold, the atomic spinor state condenses into helical patterns oriented along the pump axis \hat{x} . There is a helix at each antinode of the cavity field along \hat{y} and the phase of neighboring helices differ by π ; the resultant state is $|\psi_{\text{helix}}\rangle = |\downarrow\rangle \pm e^{ikx} \cos ky |\uparrow\rangle$, see also Ref. [34]. The broken \mathbb{Z}_2 symmetry of the phase transition is reflected in the spontaneous choice of the \pm sign, which determines the helix phase (0 or π) with respect to the phase of the pump fields.

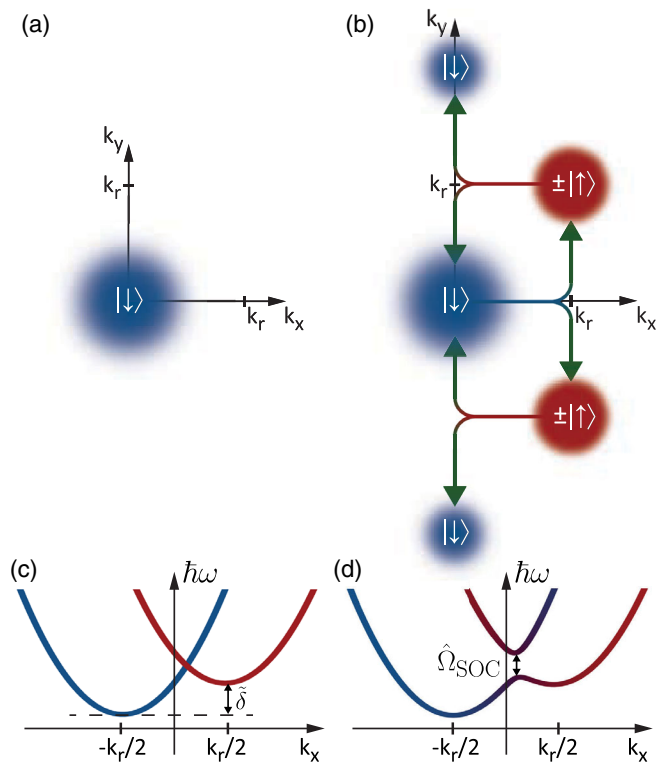


FIG. 2. (a),(b) Momentum-space depiction of the emergence of SOC. (a) Initially atoms are in a spin-polarized state $|\downarrow\rangle$. (b) If the transverse pumping strength is sufficiently strong, SOC emerges and the spin components are in different momentum states. The \pm sign of the $|\uparrow\rangle$ spin component indicates the \mathbb{Z}_2 symmetry-broken phase freedom. (c),(d) Energy-momentum dispersion relation of each spin state, transitioning from free (c) to coupled (d) dispersion bands. The coupling strength $\hat{\Omega}_{\text{SOC}}$ is proportional to \hat{a} and \hat{a}^\dagger and therefore arises dynamically as the atoms scatter pump photons into the cavity. The zero of the momentum has been shifted with respect to the lab frame by $-k_r/2$ in the plot; cf. the unitary transformations in Ref. [45].

The helix pattern serves as a grating for the Bragg diffraction (i.e., superradiant scattering) of pump photons into the cavity mode. Superradiance increases the coherent field of the cavity by a factor proportional to the number of atoms. Moreover, it locks the cavity phase to either zero or π with respect to the phase of the Raman lasers. This phase choice is correlated with the \pm sign choice in $|\psi_{\text{helix}}\rangle$.

The experiment employs two counterpropagating pump beams with amplitudes Ω_+ and Ω_- to couple two internal states $|F, m_F\rangle = |1, -1\rangle \equiv |\downarrow\rangle$ and $|F, m_F\rangle = |2, -2\rangle \equiv |\uparrow\rangle$ of a ⁸⁷Rb BEC. This is illustrated in Figs. 1(a) and 1(b). The fields induce two cavity-assisted Raman processes that together generate the Hamiltonian $\hat{H} = -\Delta_c \hat{a}^\dagger \hat{a} + \int \hat{\psi}(\mathbf{r})^\dagger \hat{H}_{\text{SOC}} \hat{\psi}(\mathbf{r}) d^3 r$. Here, Δ_c is the cavity detuning, \hat{a} (\hat{a}^\dagger) is the annihilation (creation) operator for the intracavity field, and $\hat{\psi}(\mathbf{r}) = [\hat{\psi}_\uparrow(\mathbf{r}), \hat{\psi}_\downarrow(\mathbf{r})]^T$ is a spinor containing the atomic annihilation operators $\hat{\psi}_{\uparrow\downarrow}$. The SOC Hamiltonian is

$$\hat{H}_{\text{SOC}} = \begin{bmatrix} \frac{(\hat{\mathbf{p}} + k_r/2\mathbf{e}_x)^2}{2m} + D_+ - \tilde{\delta} & \hat{\Omega}_{\text{SOC}} \cos k_r y \\ \text{H.c.} & \frac{(\hat{\mathbf{p}} - k_r/2\mathbf{e}_x)^2}{2m} + D_- \end{bmatrix}, \quad (1)$$

where k_r is the recoil momentum of the transverse pumps, \mathbf{e}_x is the unit vector in \hat{x} , $\tilde{\delta}$ is the effective two-level spin splitting set by the Raman detuning δ minus the (small) ac light shift, and $D_{\pm} = [g^2(x, z)/\Delta_{\pm}] \cos^2(k_r y) \hat{a}^\dagger \hat{a}$ is the dispersive shift [46]. The dynamical Raman coupling strength is

$$\hat{\Omega}_{\text{SOC}} = \frac{g(x, z)\Omega_+}{8\sqrt{2}\Delta_+} \hat{a}^\dagger + \frac{g(x, z)\Omega_-}{8\sqrt{2}\Delta_-} \hat{a}, \quad (2)$$

where $\Delta_+ = \Delta_- + \omega_{\text{HF}}$ and $\Delta_- \approx -112.2$ GHz are the atomic detunings for the pumps, $\omega_{\text{HF}} \approx 6.829$ GHz is the total hyperfine and Zeeman splitting between the two spin states, and $g(x, z)$ is the spatially dependent single-atom atom-cavity coupling strength. See Supplemental Material for a derivation of this SOC Hamiltonian model and its mapping to the Dicke model [45]. This model is similar to that considered in the recent proposal paper [28], where exotic Meissner-like effects were predicted to exist, as also discussed in Ref. [33]. Another recent proposal paper considered a similar Raman coupling scheme in the context of generating exotic spin Hamiltonians [34].

The SOC arises in this model because each spin state is addressed by only one of the two Raman processes. For instance, an atom in $|\downarrow\rangle$ can only scatter photons into the cavity from Ω_+ , since Ω_- is off resonance by $\approx 2\omega_{\text{HF}}$. Because of the running-wave nature of the transverse pumps, each scattering event imparts a net momentum along $+\mathbf{e}_x$ onto the atom, because the accompanying momentum change $\pm k_r$ along the cavity direction averages to zero, since either direction is equally probable. Likewise, an atom originating in $|\uparrow\rangle$ will receive a net momentum kick along $-\mathbf{e}_x$, where the direction is opposite due to the counterpropagating orientation of the running-wave pump beams. The result—opposite spin states moving in opposite directions—thus realizes SOC. Note, however, that the Raman coupling term $\hat{\Omega}_{\text{SOC}}$ contains the cavity-field operators \hat{a} and \hat{a}^\dagger . Since the cavity field is determined self-consistently by the dynamics of the atom-spin-cavity system and is initially in a vacuum state, the SOC term emerges *dynamically* as the atoms organize to scatter superradiantly.

We now present data demonstrating emergent SOC. A BEC of $4.1(3) \times 10^5$ ^{87}Rb atoms, all prepared in $|\downarrow\rangle$, is placed at the center of a TEM_{00} cavity by an optical dipole trap; see Supplemental Material for more experimental details [45]. The cavity and pump fields are tuned such that $\Delta_c = -10$ MHz and $\delta = -6$ kHz. We record the light emitted from the cavity on a single-photon counter. The power of the transverse pumps is gradually increased, shown by the black dashed line in Fig. 3(a). The recorded

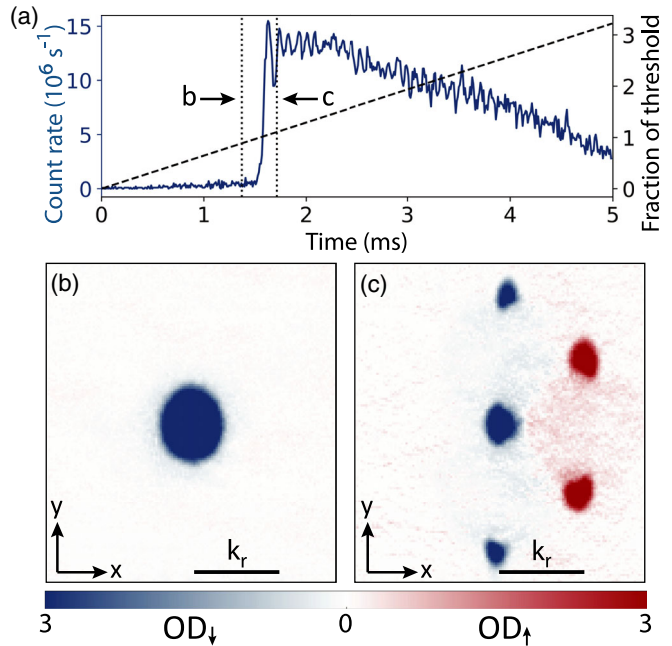


FIG. 3. (a) Cavity emission detected by single-photon counters (solid blue line) and optical power in the Raman beams (dashed black line), both as a function of time. Steady-state SOC persists up to a few milliseconds; oscillations are due to system dynamics as described in Ref. [49]. (b),(c) Spin-resolved momentum distribution in time of flight, taken at the points labeled in (a). All atoms are in $|\downarrow\rangle$ just below threshold (b). Above threshold (c), spin-up atoms have acquired a net momentum in the x direction, as shown by the spin-colored Bragg peaks at nonzero momentum. Also shown are second-order diffraction peaks along the cavity direction due to the reverse Raman process.

cavity emission is shown in blue and rapidly increases when the optical power reaches threshold, indicating the emergence of superradiant scattering and, consequently, the nonzero Raman coupling needed for SOC [47]. Fast, ~ 10 kHz, oscillations in the cavity output can be seen. These are due to intrinsic dynamics of the cavity and spin-helix mode: The spin-helix polariton mode becomes populated above threshold and executes small oscillations before settling into the new superradiant steady state, aided by the cavity dissipation. The cavity field adapts to the change in the spin-helix mode population, signifying the dynamic nature of the spin-orbit coupling term. The superradiance lifetime is presumably limited by the dephasing of the two pumping beams, which we independently verified is also on the few-millisecond timescale.

We can compare the observed and predicted thresholds for the Dicke model. See Supplemental Material for a discussion of the threshold prediction [45]. The pump strengths at threshold $\eta_D \equiv [\sqrt{N}g(x, z)\Omega_+/8\sqrt{2}\Delta_+] = [\sqrt{N}g(x, z)\Omega_-/8\sqrt{2}\Delta_-]$ are measured through microwave spectroscopy on the $|\uparrow\rangle \leftrightarrow |\downarrow\rangle$ transition. At the point when the SOC threshold is crossed, $\eta_D = 128(4)$ kHz, whereas the prediction is $\eta_D = 129.9(3)$ kHz. These

results are in good agreement and comparable to experiments realizing Dicke models in other contexts [48]. From this pump strength and the detected cavity emission, we can estimate the strength of the SOC term, per Eq. (2). We reiterate that this is a dynamical quantity; i.e., its magnitude depends on the intracavity field. Averaging over a 0.5-ms interval about the 2-ms mark in Fig. 3(a), the inferred intracavity-field occupation number is $\langle \hat{a}^\dagger \hat{a} \rangle = 1.7(1) \times 10^2$. As a result, the Raman coupling strength rises from zero before threshold to $\langle \hat{\Omega}_{\text{SOC}} \rangle = 2.2(1)E_r$ at $t=2\text{ ms}$.

We have observed that the SOC-induced Bragg peaks emerge at the same pump power as the threshold for superradiant cavity emission, as expected; see Fig. 2. This is determined by correlating the cavity emission signal in Fig. 3(a) with the spin-resolved, time-of-flight imaging of the atomic gas in Figs. 3(b) and 3(c) [50]. These images provide full information about each spin species' momentum distribution. Below threshold, the cavity emission is low and all atoms are in the initial state, i.e., a zero-momentum spin-polarized state. This is shown in Fig. 3(b). At a time shortly after reaching threshold, when emission has jumped to a higher rate, a fraction of the atoms have undergone a spin flip and have scattered into the two Bragg peaks at $(k_r, \pm k_r)$, as shown in Fig. 3(c). Additionally, the reverse process occurs, mediated by Ω_- , transferring atoms from these two Bragg peaks into $(0, \pm 2k_r)$ as well as repopulating the zero-momentum component [51]. Crucially, the spin species have now separated in momentum space, with a net difference in momentum component along \mathbf{e}_x .

To demonstrate the \mathbb{Z}_2 symmetry breaking of the $|\psi_{\text{helix}}\rangle$ state, we repeatedly ramp into and out of the SOC phase, akin to previous experiments [52,53], while observing the cavity emission with a phase-sensitive heterodyne detector. The local oscillator is set to the average frequency of the two Raman beams [43]. Figures 4(a) and 4(b) show the ramp profile and the amplitude and phase of the cavity output, respectively. While our setup is not phase stable from shot to shot due to long-term mechanical drifts, phase stability is maintained during the short-term transverse pumping portion of the sequence. This allows us to observe the relative phase between subsequent superradiant pulses, which for a spontaneously broken \mathbb{Z}_2 symmetry should be evenly distributed between zero and π . A histogram of phase differences is shown in Fig. 4(c) for 310 experimental trials and a clear bifurcation between zero and π can be seen. The number of phase differences around zero (π) is 510 (513), which implies that the *a posteriori* estimate for consecutive superradiant pulses possessing the same phase is 49.9(1.6)%; i.e., their phases are statistically independent, demonstrating the breaking of a \mathbb{Z}_2 symmetry.

The observed momentum distribution taken together with the measurement of symmetry breaking is evidence that the spin state corresponds to the aforementioned spinor-helix state $|\psi_{\text{helix}}\rangle$. This state possesses similarities

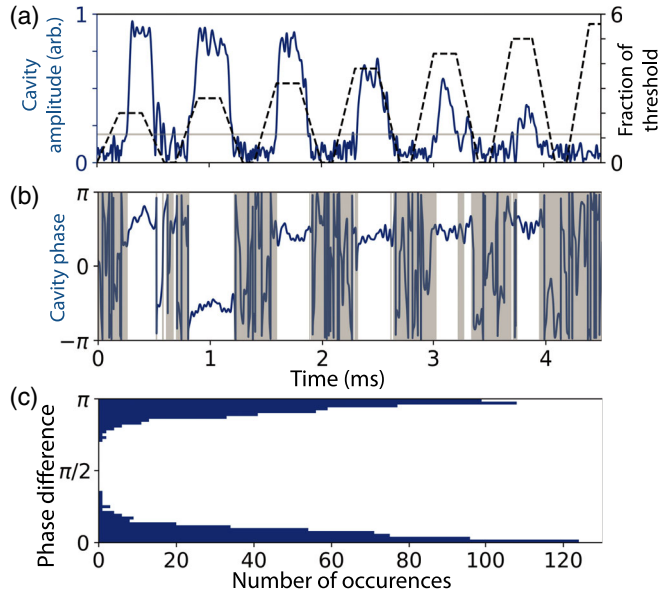


FIG. 4. (a) Cavity emission amplitude (solid blue line) and transverse pump power expressed as a multiple of the threshold power (dashed black line), both as a function of time. (b) Phase of the cavity emission, as observed with heterodyne detection. Six superradiant pulses can be seen, each with freely chosen 0 or π phase (up to an irrelevant global phase). Shading is applied when the cavity amplitude is less than 25% of the peak value, indicated by the gray horizontal line in (a) and distinguishes between the phase locked (superradiant) and unlocked (normal) phases. (c) Histogram of phase differences between consecutive pulses, for a total of 310 experiments. The imbalance between zero versus π is 0.3%.

to the persistent spin-helix state observed in semiconductors [54,55] and could be extended to Abelian or non-Abelian ‘Majorana’ spinor-helix states through the use of high-spin lanthanide atoms such as dysprosium (on time-scales less than that set by dipolar relaxation) [41,56–58]. The limited superradiance lifetime hampered our ability to measure both the excitation spectrum of the spinor-helix mode and the position of the SOC band minima in Fig. 2(d) versus the emergent Raman coupling strength. Future improvements to the Raman laser lock should improve this lifetime and enable these measurements.

In conclusion, we have observed spin-orbit coupling that emerges through a process of spin-spatial (spinor) self-organization. This organization arises due to the scattering of running-wave pump fields into the cavity field. Quantum fluctuations of the cavity field stimulate this scattering process, generating a cavity field incoherent with the pump field. At higher pump power, a runaway self-organization transition induces the superradiant scattering of a field whose phase is locked with the pumps. The resulting coherent Raman coupling—arising from the mutually coherent pump and cavity fields—induces dynamical SOC. Moreover, the BEC-cavity QED system is strongly coupled and therefore quantum fluctuations can play a role

in the SOC dynamics. This is because the spin-spatial self-organization takes place at a SOC threshold corresponding to only a few cavity photons wherein quantum fluctuations are non-negligible. Consequences of this will be explored in future work.

The addition of dynamical SOC to the toolbox of quantum simulation in the nonequilibrium context opens new avenues for the exploration of a wide range of phenomena in quantum gases, e.g., topological superradiant superfluids. Moreover, dynamical artificial gauge fields can be created by a simple modification of the present experiment. Specifically, by using a multimode cavity (possible with our present apparatus [59]) and by choosing the pump laser frequencies to enhance the effects of their differential dispersive light shift on the spin states, Meissner-like effects can be observed [33]. We speculate that, with dynamical gauge fields, combined with the strong, sign-changing, and tunable-range photon-mediated interactions provided by multimode cavities [9–11], quantum simulators will be able to create a wide variety of exotic, nonequilibrium quantum matter.

We thank Jonathan Keeling and Sarang Gopalakrishnan for helpful discussions. We are grateful for funding support from the Army Research Office.

-
- [1] I. B. Spielman, Raman processes and effective gauge potentials, *Phys. Rev. A* **79**, 063613 (2009).
- [2] J. Dalibard, F. Gerbier, G. Juzeliūnas, and P. Öhberg, Colloquium: Artificial gauge potentials for neutral atoms, *Rev. Mod. Phys.* **83**, 1523 (2011).
- [3] N. Goldman, G. Juzeliūnas, P. Öhberg, and I. B. Spielman, Light-induced gauge fields for ultracold atoms, *Rep. Prog. Phys.* **77**, 126401 (2014).
- [4] Y. J. Lin, K. Jiménez-García, and I. B. Spielman, Spin-orbit-coupled Bose-Einstein condensates, *Nature (London)* **471**, 83 (2011).
- [5] L. Jiang, T. Kitagawa, J. Alicea, A. R. Akhmerov, D. Pekker, G. Refael, J. I. Cirac, E. Demler, M. D. Lukin, and P. Zoller, Majorana Fermions in Equilibrium and in Driven Cold-Atom Quantum Wires, *Phys. Rev. Lett.* **106**, 220402 (2011).
- [6] J. Ruhman, E. Berg, and E. Altman, Topological States in a One-Dimensional Fermi Gas with Attractive Interaction, *Phys. Rev. Lett.* **114**, 100401 (2015).
- [7] H. J. Kimble, Strong interactions of single atoms, and photons in cavity QED, *Phys. Scr.* **T76**, 127 (1998).
- [8] H. Ritsch, P. Domokos, F. Brennecke, and T. Esslinger, Cold atoms in cavity-generated dynamical optical potentials, *Rev. Mod. Phys.* **85**, 553 (2013).
- [9] V. D. Vaidya, Y. Guo, R. M. Kroeze, K. E. Ballantine, A. J. Kollár, J. Keeling, and B. L. Lev, Tunable-Range, Photon-Mediated Atomic Interactions in Multimode Cavity QED, *Phys. Rev. X* **8**, 011002 (2018).
- [10] Y. Guo, R. M. Kroeze, V. D. Vaidya, J. Keeling, and B. L. Lev, Sign-Changing Photon-Mediated Atom Interactions in Multimode Cavity Quantum Electrodynamics, *Phys. Rev. Lett.* **122**, 193601 (2019).
- [11] Y. Guo, V. D. Vaidya, R. M. Kroeze, R. A. Lunney, B. L. Lev, and J. Keeling, Emergent and broken symmetries of atomic self-organization arising from Gouy phase shifts in multimode cavity QED, *Phys. Rev. A* **99**, 053818 (2019).
- [12] S. Diehl, A. Tomadin, A. Micheli, R. Fazio, and P. Zoller, Dynamical Phase Transitions and Instabilities in Open Atomic Many-Body Systems, *Phys. Rev. Lett.* **105**, 015702 (2010).
- [13] L. M. Sieberer, S. D. Huber, E. Altman, and S. Diehl, Dynamical Critical Phenomena in Driven-Dissipative Systems, *Phys. Rev. Lett.* **110**, 195301 (2013).
- [14] L. M. Sieberer, M. Buchhold, and S. Diehl, Keldysh field theory for driven open quantum systems, *Rep. Prog. Phys.* **79**, 096001 (2016).
- [15] P. Kirton, M. M. Roses, J. Keeling, and E. G. Dalla Torre, Introduction to the Dicke Model: From equilibrium to nonequilibrium, and vice versa, *Adv. Quantum Technol.* **2**, 1800043 (2018).
- [16] F. Mivehvar and D. L. Feder, Synthetic spin-orbit interactions and magnetic fields in ring-cavity QED, *Phys. Rev. A* **89**, 013803 (2014).
- [17] Y. Deng, J. Cheng, H. Jing, and S. Yi, Bose-Einstein Condensates with Cavity-Mediated Spin-Orbit Coupling, *Phys. Rev. Lett.* **112**, 143007 (2014).
- [18] B. Padhi and S. Ghosh, Spin-orbit-coupled Bose-Einstein condensates in a cavity: Route to magnetic phases through cavity transmission, *Phys. Rev. A* **90**, 023627 (2014).
- [19] L. Dong, L. Zhou, B. Wu, B. Ramachandran, and H. Pu, Cavity-assisted dynamical spin-orbit coupling in cold atoms, *Phys. Rev. A* **89**, 011602(R) (2014).
- [20] L. Dong, C. Zhu, and H. Pu, Photon-induced spin-orbit coupling in ultracold atoms inside optical cavity, *Atoms* **3**, 182 (2015).
- [21] F. Mivehvar and D. L. Feder, Enhanced stripe phases in spin-orbit-coupled Bose-Einstein condensates in ring cavities, *Phys. Rev. A* **92**, 023611 (2015).
- [22] C. Zhu, L. Dong, and H. Pu, Effects of spin-orbit coupling on Jaynes-Cummings and Tavis-Cummings models, *Phys. Rev. A* **94**, 053621 (2016).
- [23] C. Kollath, A. Sheikhan, S. Wolff, and F. Brennecke, Ultracold Fermions in a Cavity-Induced Artificial Magnetic Field, *Phys. Rev. Lett.* **116**, 060401 (2016).
- [24] A. Sheikhan, F. Brennecke, and C. Kollath, Cavity-induced chiral states of fermionic quantum gases, *Phys. Rev. A* **93**, 043609 (2016).
- [25] W. Zheng and N. R. Cooper, Superradiance Induced Particle Flow via Dynamical Gauge Coupling, *Phys. Rev. Lett.* **117**, 175302 (2016).
- [26] A. Sheikhan, F. Brennecke, and C. Kollath, Cavity-induced generation of nontrivial topological states in a two-dimensional Fermi gas, *Phys. Rev. A* **94**, 061603(R) (2016).
- [27] C.-M. Halati, A. Sheikhan, and C. Kollath, Cavity-induced artificial gauge field in a Bose-Hubbard ladder, *Phys. Rev. A* **96**, 063621 (2017).
- [28] C.-M. Halati, A. Sheikhan, and C. Kollath, Cavity-induced spin-orbit coupling in an interacting bosonic wire, *Phys. Rev. A* **99**, 033604 (2019).

- [29] The ring cavity proposals [16,19–22] induce SOC by directly driving the cavity modes with coherent fields. This fixes the relative phase of the driving fields at any field strength. By contrast, the Fabry-Perot cavity proposals [17,18,23–28], including this work, allow the cavity field to be populated from vacuum through a scattering process where phase locking (and hence Raman coupling) emerges dynamically.
- [30] L. W. Clark, B. M. Anderson, L. Feng, A. Gaj, K. Levin, and C. Chin, Observation of Density-Dependent Gauge Fields in a Bose-Einstein Condensate Based on Micromotion Control in a Shaken Two-Dimensional Lattice, *Phys. Rev. Lett.* **121**, 030402 (2018).
- [31] F. Görg, K. Sandholzer, J. Minguzzi, R. Desbuquois, M. Messer, and T. Esslinger, Realization of density-dependent Peierls phases to engineer quantized gauge fields coupled to ultracold matter, *Nat. Phys.*, <https://doi.org/10.1038/s41567-019-0615-4> (2019).
- [32] K. A. Yasir, L. Zhuang, and W.-M. Liu, Spin-orbit-coupling-induced backaction cooling in cavity optomechanics with a Bose-Einstein condensate, *Phys. Rev. A* **95**, 013810 (2017).
- [33] K. E. Ballantine, B. L. Lev, and J. Keeling, Meissner-like Effect for a Synthetic Gauge Field in Multimode Cavity QED, *Phys. Rev. Lett.* **118**, 045302 (2017).
- [34] F. Mivehvar, H. Ritsch, and F. Piazza, Cavity-Quantum-Electrodynamical Toolbox for Quantum Magnetism, *Phys. Rev. Lett.* **122**, 113603 (2019).
- [35] J.-S. Pan, X.-J. Liu, W. Zhang, W. Yi, and G.-C. Guo, Topological Superradiant States in a Degenerate Fermi Gas, *Phys. Rev. Lett.* **115**, 045303 (2015).
- [36] D. Yu, J.-S. Pan, X.-J. Liu, W. Zhang, and W. Yi, Topological superradiant state in Fermi gases with cavity induced spin-orbit coupling, *Front. Phys.* **13**, 136701 (2018).
- [37] Z. Zheng, X.-B. Zou, and G.-C. Guo, Synthetic topological Kondo insulator in a pumped optical cavity, *New J. Phys.* **20**, 023039 (2018).
- [38] Z. Wu, L. Zhang, W. Sun, X.-T. Xu, B.-Z. Wang, S.-C. Ji, Y. Deng, S. Chen, X.-J. Liu, and J.-W. Pan, Realization of two-dimensional spin-orbit coupling for Bose-Einstein condensates, *Science* **354**, 83 (2016).
- [39] P. Wang, Z.-Q. Yu, Z. Fu, J. Miao, L. Huang, S. Chai, H. Zhai, and J. Zhang, Spin-Orbit Coupled Degenerate Fermi Gases, *Phys. Rev. Lett.* **109**, 095301 (2012).
- [40] L. W. Cheuk, A. T. Sommer, Z. Hadzibabic, T. Yefsah, W. S. Bakr, and M. W. Zwierlein, Spin-Injection Spectroscopy of a Spin-Orbit Coupled Fermi Gas, *Phys. Rev. Lett.* **109**, 095302 (2012).
- [41] N. Q. Burdick, Y. Tang, and B. L. Lev, Long-Lived Spin-Orbit-Coupled Degenerate Dipolar Fermi Gas, *Phys. Rev. X* **6**, 031022 (2016).
- [42] For standing-wave pumps, the resulting state of spinful atoms in a BEC has been experimentally shown to be a “spinor polariton condensate,” i.e., a jointly organized spin *and* spatial light-matter state of macroscopic population [43]. While the $k = 0$ ground state of the BEC is necessary for macroscopic population of the ground and first excited momentum states, the broken U(1) gauge symmetry of the BEC is not relevant.
- [43] R. M. Kroese, Y. Guo, V. D. Vaidya, J. Keeling, and B. L. Lev, Spinor Self-Ordering of a Quantum Gas in a Cavity, *Phys. Rev. Lett.* **121**, 163601 (2018).
- [44] Checkerboard density-wave organization also arises in running-wave-pumped cavities, see K. J. Arnold, M. P. Baden, and M. D. Barrett, Self-Organization Threshold Scaling for Thermal Atoms Coupled to a Cavity, *Phys. Rev. Lett.* **109**, 153002 (2012).
- [45] See Supplemental Material at <http://link.aps.org-supplemental/10.1103/PhysRevLett.123.160404> for a derivation and discussion of the Hamiltonian.
- [46] Since the differential dispersive shift is small compared to the other terms, we will neglect it from here forward.
- [47] We note that the duration of emission is longer than that from a single spin-flip process [48], implying steady-state SOC instead of transient effects.
- [48] Z. Zhang, C. H. Lee, R. Kumar, K. J. Arnold, S. J. Masson, A. L. Grimsmo, A. S. Parkins, and M. D. Barrett, Dicke-model simulation via cavity-assisted Raman transitions, *Phys. Rev. A* **97**, 043858 (2018).
- [49] M. J. Bhaseen, J. Mayoh, B. D. Simons, and J. Keeling, Dynamics of nonequilibrium Dicke models, *Phys. Rev. A* **85**, 013817 (2012).
- [50] See Ref. [43] for how spin-resolved imaging is performed in our apparatus.
- [51] These secondary diffraction peaks do not occur in a single spin-flip process.
- [52] K. Baumann, R. Mottl, F. Brennecke, and T. Esslinger, Exploring Symmetry Breaking at the Dicke Quantum Phase Transition, *Phys. Rev. Lett.* **107**, 140402 (2011).
- [53] A. J. Kollár, A. T. Papageorge, V. D. Vaidya, Y. Guo, J. Keeling, and B. L. Lev, Supermode-density-wave-polariton condensation with a Bose-Einstein condensate in a multimode cavity, *Nat. Commun.* **8**, 14386 (2017).
- [54] B. A. Bernevig, J. Orenstein, and S.-C. Zhang, Exact SU(2) Symmetry and Persistent Spin Helix in a Spin-Orbit Coupled System, *Phys. Rev. Lett.* **97**, 236601 (2006).
- [55] J. D. Koralek, C. P. Weber, J. Orenstein, B. A. Bernevig, S.-C. Zhang, S. Mack, and D. D. Awschalom, Emergence of the persistent spin helix in semiconductor quantum wells, *Nature (London)* **458**, 610 (2009).
- [56] B. Lian, T.-L. Ho, and H. Zhai, Searching for non-Abelian phases in the Bose-Einstein condensate of dysprosium, *Phys. Rev. A* **85**, 051606(R) (2012).
- [57] X. Cui, B. Lian, T.-L. Ho, B. L. Lev, and H. Zhai, Synthetic gauge field with highly magnetic lanthanide atoms, *Phys. Rev. A* **88**, 011601(R) (2013).
- [58] N. Q. Burdick, K. Baumann, Y. Tang, M. Lu, and B. L. Lev, Fermionic Suppression of Dipolar Relaxation, *Phys. Rev. Lett.* **114**, 023201 (2015).
- [59] A. J. Kollár, A. T. Papageorge, K. Baumann, M. A. Armen, and B. L. Lev, An adjustable-length cavity and Bose-Einstein condensate apparatus for multimode cavity QED, *New J. Phys.* **17**, 043012 (2015).